

Support information

Determining Fatigue Threshold of Elastomer through Elastic Limit Strain Point

Xinglinmao Li ^a, Wen Li ^{ab*}, Jia Cheng ^a, Xiao Sun ^a, Yue Zhang ^{ab}, Chunping Xiang ^c,
Shougang Chen ^{ab*}

a: School of Materials Science and Engineering, Ocean University of China, Qingdao,
266100, PR China

b: Qingdao Key Laboratory of Marine Extreme Environmental Materials, Qingdao,
266100, PR China

c: School of Engineering, Ocean University of China, Qingdao, 266100, PR China

Corresponding Authors

* Wen Li liwen3710@ouc.edu.cn

* Shougang Chen sgchen@ouc.edu.cn

SI1. The shape and size of the sample used for mechanical property testing

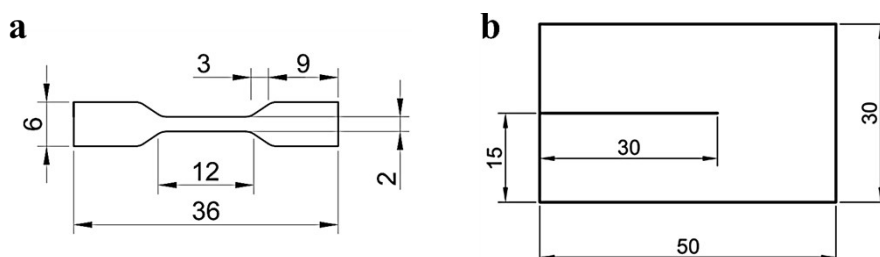


Figure. S1 The shape and size of the sample used for mechanical property testing

SI2. Density diagram

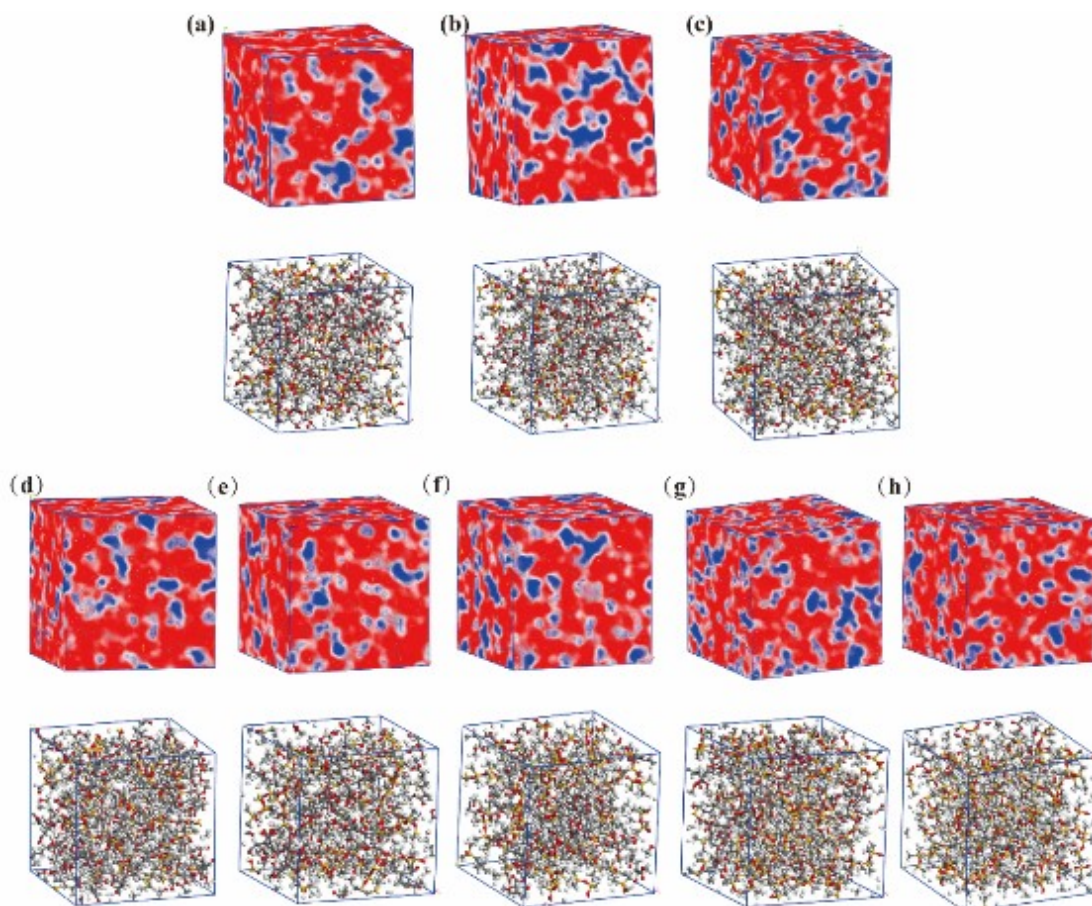


Figure.S2 density diagram of the system with different branch chain lengths, and the corresponding equilibrium configuration. (a) PDMS-PMA (b)PDMS-PEA and (c)PDMS-PnBA (d) PMA: peptone = 2: 8, (e) 4: 6 (f) 6: 4 (g) 8: 2 and (h) 10: 0

SI3. Material characterization

SI3.1. Scanning electron microscope and Energy Dispersive Spectroscopy

The morphology of the hydrogel was observed through scanning electron microscopy (SEM, Phenom ProX, China) at an accelerating voltage of 10 kV. The gold-sputtering procedure was carried out before the SEM test.

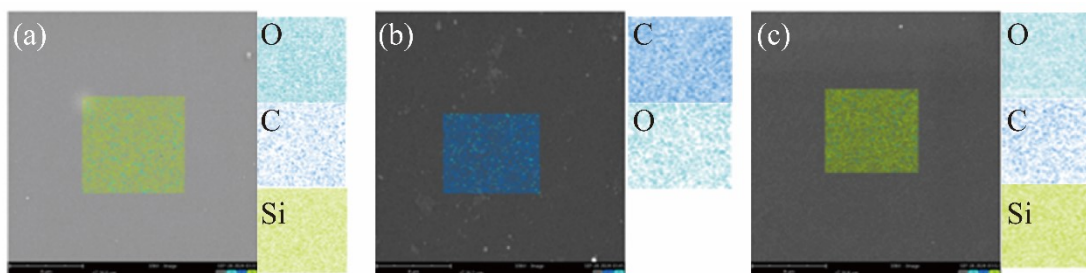


Figure. S3 EDS of PMA (a), PDMS (b) and IDNE (c)

Table S1. Element atomic Conc. and weight Conc. in three elastomers

	Oxygen		Carbon		Silicon	
	Atomic Conc.	Weight Conc.	Atomic Conc.	Weight Conc.	Atomic Conc.	Weight Conc.
PMA	42.95	39.30	33.64	23.11	23.41	37.59
PDMS	21.95	27.25	78.05	72.75		
IDNS	42.33	39.04	34.98	24.22	22.69	36.74

SI3.2. FT-IR; TGA and water absorption

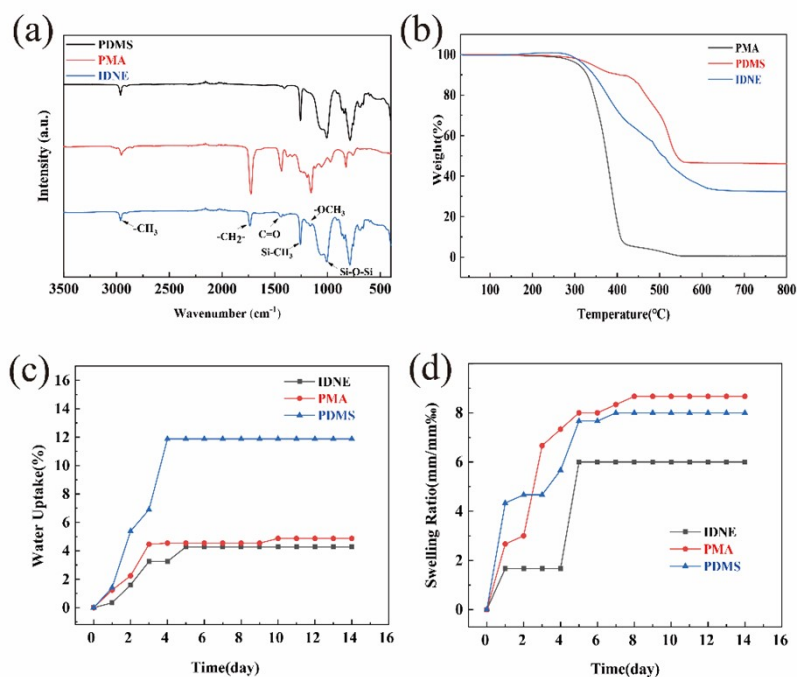


Figure. S4 (a), the infrared spectra of PMA, PDMS, and IDNE (b) The thermal gravimetric analysis (TGA) curves of PMA, PDMS, and IDNE (c) Water absorption of PMA, PDMS and IDNE; (d) Swelling rate of PMA, PDMS and IDNE

The FTIR spectroscopy results shown in **Figure.S4 (a)** indicate the presence of specific functional groups in PMA, PDMS, and IDNE. In PMA, the asymmetric stretching of $-\text{CH}_3$ is observed at 2964 cm^{-1} , which is also present in IDNE. In PDMS, absorption peaks for $-\text{CH}_2-$ appear at 1740 cm^{-1} , $\text{Si}-\text{CH}_3$ at 1255 cm^{-1} , and $\text{Si}-\text{O}-\text{Si}$ at 1012 cm^{-1} , all of which are also observed in IDNE. Additionally, the $\text{C}=\text{O}$ stretching in PMA is observed at 1443 cm^{-1} , and the asymmetric bending of $\text{O}-\text{CH}_3$ is observed at 1158 cm^{-1} , which are also present in IDNE. Based on these FTIR results, it can be concluded that IDNE is composed of a dual-network structure consisting of PDMS and PMA. The presence of similar absorption peaks in both IDNE and the individual components (PDMS and PMA) suggests the incorporation of their respective functional groups in the IDNE material. The thermal gravimetric analysis (TGA) was conducted in air with a heating rate of 10 k per minute, starting from $25\text{ }^\circ\text{C}$ and heating up to $800\text{ }^\circ\text{C}$, to determine the thermal stability of the coating. The TGA results are shown in **Figure.S4(b)**. In the TGA curve, it can be observed that the mass loss of PMA begins at around $300\text{ }^\circ\text{C}$, and by $400\text{ }^\circ\text{C}$, approximately 90% of the sample's mass has been lost. This significant mass loss is primarily due to the degradation of the PMA molecular network through oxidative chain scission reactions at high temperatures in the presence of oxygen.

For IDNE, the rapid mass loss starts at around $300\text{ }^\circ\text{C}$, and the rate of mass loss slows down at $400\text{ }^\circ\text{C}$. This is because the mass loss of PMA in the composite material is completed at this temperature. After $600\text{ }^\circ\text{C}$, the mass loss of IDNE tends to stabilize, and the remaining mass is attributed to the inorganic silicon products formed from the

combustion of the PDMS segments in IDNE. The TGA (TGA-5500, TA Instruments, Inc., Switzerland) results confirm the successful synthesis of IDNE from the two materials, as the mass loss only occurs at high temperatures around 300 °C. The mass loss during the heating process is relatively stable, indicating good thermal stability during use.

To test the water absorption performance of the materials, they were cut into circular shapes with a diameter of 1cm and immersed in sealed bottles containing water solution to ensure uniform absorption. The weight of the expanded network of different materials was recorded until a constant weight was observed. The experiment lasted for 15 days. The swelling ratio of the three different materials was calculated using the Formula S1, as shown in **Figure S4(c)(d)**. It can be seen that IDNE exhibits the lowest swelling ratio. The water absorption rate is shown in **Figure S4 (d)**, with IDNE having a water absorption rate of only 4%. This is because the introduction of the dual-network structure with PMA makes the material more compact, with a tighter surface structure and stronger hydrophobicity, making it difficult for water molecules to adhere or enter the material.

$$G=(G2-G1)/G1*100\% \qquad \text{Formula. S1}$$

SI3.3. Visual photos of PMA, PDMS and IDNE

We can intuitively see the obvious difference in light transmittance between the three materials. Because the IDNE material has a higher density, its light transmittance is relatively weak.

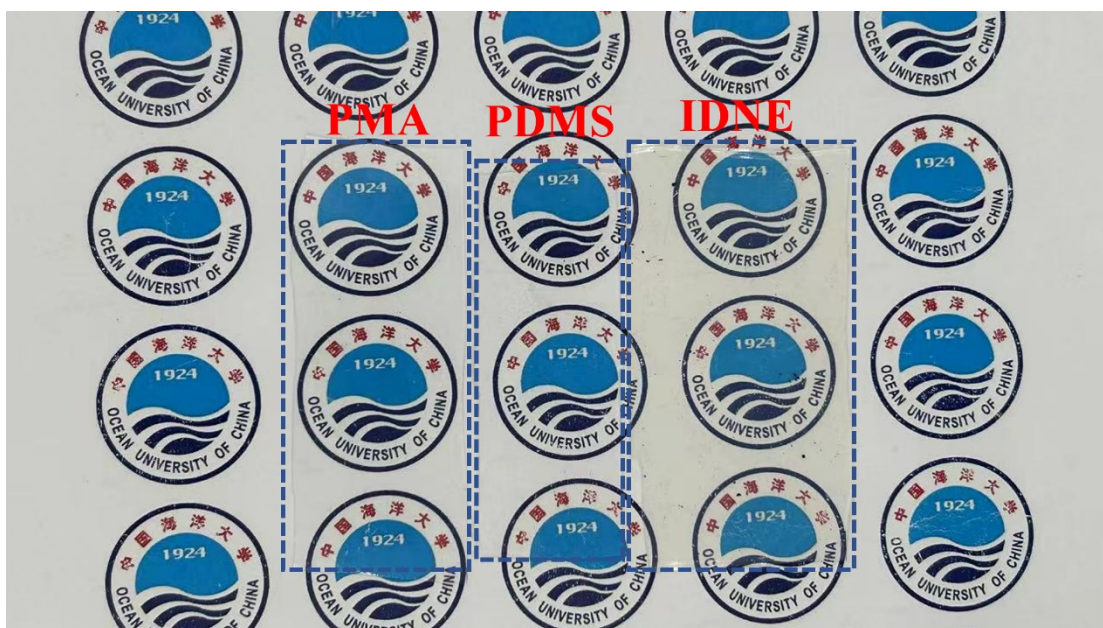


Figure. S5 Visual photos of PMA, PDMS and IDNE

SI3.4. Antifouling performance test of IDNE

The strain used in the experiment was *Staphylococcus aureus* (RiShui Biotech Co. Ltd. (Qingdao, China)) (*S. aureus*) to test the antibacterial and anti-adhesion properties of the tested material. Firstly, 0.5 g of peptone, 0.25 g of sodium chloride (Sinopharm Chemical Regent Co., Ltd (Shanghai, China)) (NaCl) and 0.25 g of yeast extract were weighed and placed into a conical flask. Then, 50 mL of deionized water was added, and the conical flask was sonicated and stirred until fully dissolved. After that, the conical flask with the pale-yellow solution was placed into a sterilization pot. The sterilization pot was heated to 121 °C and sterilized for 30 minutes. After the sterilization was completed, the sterilization pot was allowed to cool down to room temperature. The conical flask with the solution was then placed into a super clean bench, and the ultraviolet lamp was turned on to irradiate the solution for 30 minutes before proceeding to the next step. 50 μ L of *S. aureus* frozen liquid was taken using a pipette gun and added to the prepared culture medium. Then, the mixture was placed in

a constant temperature shaking incubator at 37 °C with a shaking speed of 110 rpm and incubated for 24 hours to obtain a concentrated bacterial suspension with a concentration of approximately 10^9 CFU mL⁻¹.

The bacterial liquid cultivated in the constant temperature and humidity chamber for 24 hours was taken out and sequentially diluted with ultrapure water to a concentration of 10^4 CFU mL⁻¹ for subsequent fluorescence analysis. The elastic material was cut into squares with a size of 20 mm × 20 mm × 0.5 mm (length × width × thickness) and soaked in the bacterial liquid with a concentration of 10^4 CFU mL⁻¹ for 24 hours. To reduce errors, three samples of each type were soaked. After 24 hours, some of the samples were stained with live-dead bacteria dye. The samples were placed flat on a microscope slide, and the dye was dropped onto the samples. Then, a cover slide was placed on top, and the samples were stained in the dark for 15 minutes. The live bacteria were stained green, and the dead bacteria were stained red. The samples were observed under a fluorescence microscope, the field of view was adjusted, and the fluorescence images were saved. Another part of the samples was taken out, rinsed with simulated seawater, and then stained with a live-dead bacteria dye. The samples were placed flat on a microscope slide, and the dye was dropped onto the samples. Then, excess liquid was removed using a lens cleaning paper, and the samples were stained in the dark for 15 minutes. The live bacteria were stained green, and the dead bacteria were stained red. The samples were observed under a fluorescence microscope, the field of view was adjusted, and the fluorescence images were saved.

SI4. Mullins testing- 24 hours interval between the two loading processes

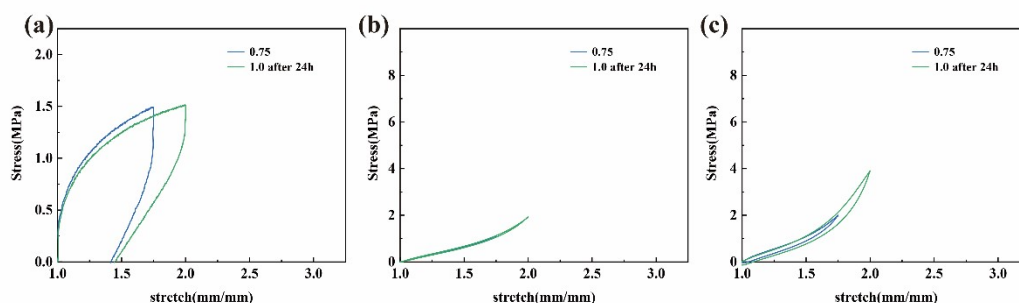


Figure. S6 24 hours interval between the two loading processes of PMA(a), PDMS(b) and IDNE (c)

SI5. Mullins testing- Hysteresis values (%)

Table S2. Data table of hysteresis values obtained from Mullins mechanical tests of PDMS

	0.25	0.5	0.75	1	1.25	1.5	1.75	2	2.5	3	4
3:1	0.0417	0.0326	0.0011	0.0050	0.0204	0.0804					
7:1	0.0239	0.0154	0.0171	0.0304							
10:1	0.0362	0.0226	0.0171	0.0249							
15:1	0.0425	0.0270	0.0164	0.0101	0.0100	0.0142	0.0168				
20:1	0.0627	0.0233	0.0072	0.0090	0.0154	0.0004	0.0121	0.0108	0.0514	0.0928	0.3372

SI6. The calculation of the energy release rate

In defining the energy release rate, however, we ignore the presence of inelasticity, regard the entire sample with a precut crack as an elastic body, all the way to the crack front. Denote the elastic energy of the body by U . The area of the crack, A , is measured when the body is in the undeformed state. The body is subject to an applied force F and displacement Δ . When

the displacement changes by $d\Delta$, the applied force does work $Fd\Delta$. The elastic energy of the body in the deformed state is a function of the displacement and the crack area, $U(\Delta, A)$, and is the area under the force displacement curve when the area of crack is fixed. The energy release rate G is defined by the equation $Fd\Delta = dU + GdA$. Thus, $F = \partial U(\Delta, A) / \partial \Delta$ and $G = -\partial U(\Delta, A) / \partial A$. The energy release rate has the unit of energy per unit area.

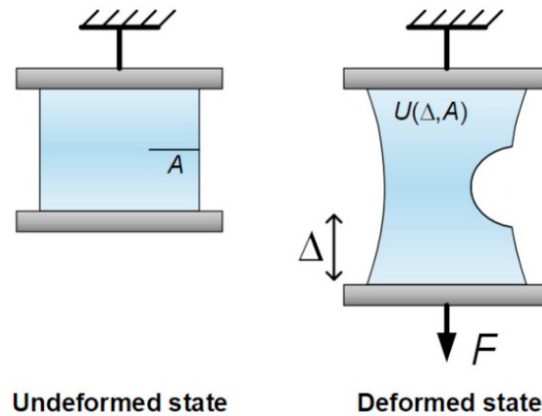


Figure. S7 A body has a crack of area A measured in the undeformed state. The body is subject to an applied force F and displacement Δ . The elastic energy of the body in the deformed state is a function of the displacement and the crack area, $U(\Delta, A)$.

The energy release rate is a loading parameter, not a material property. In defining G , we picture two bodies identical in every other way, except for a slight difference in the areas of the precut cracks when the bodies are in the undeformed states, A' and A'' . Both cracks are precut using, say, a razor blade. When the bodies are loaded, the precut cracks do not grow. The energy release rate is $G = - [U(\Delta, A'') - U(\Delta, A')] / (A'' - A')$. The energy release rate is fully determined by the elastic boundary value problems associated with the two bodies, and requires no information of fracture.

SI7. Strength and toughness of different double network structure and ratios

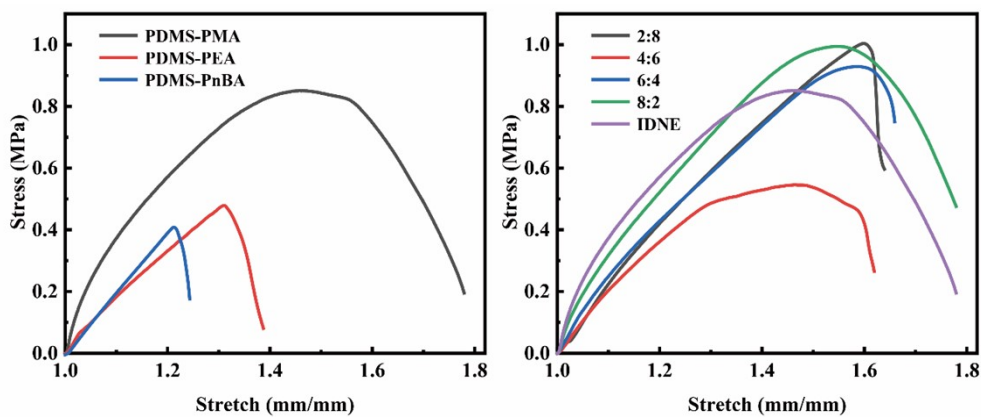


Figure. S8. S-S curve of PDMS and IDNE with pre-crack in different double network structure and ratios

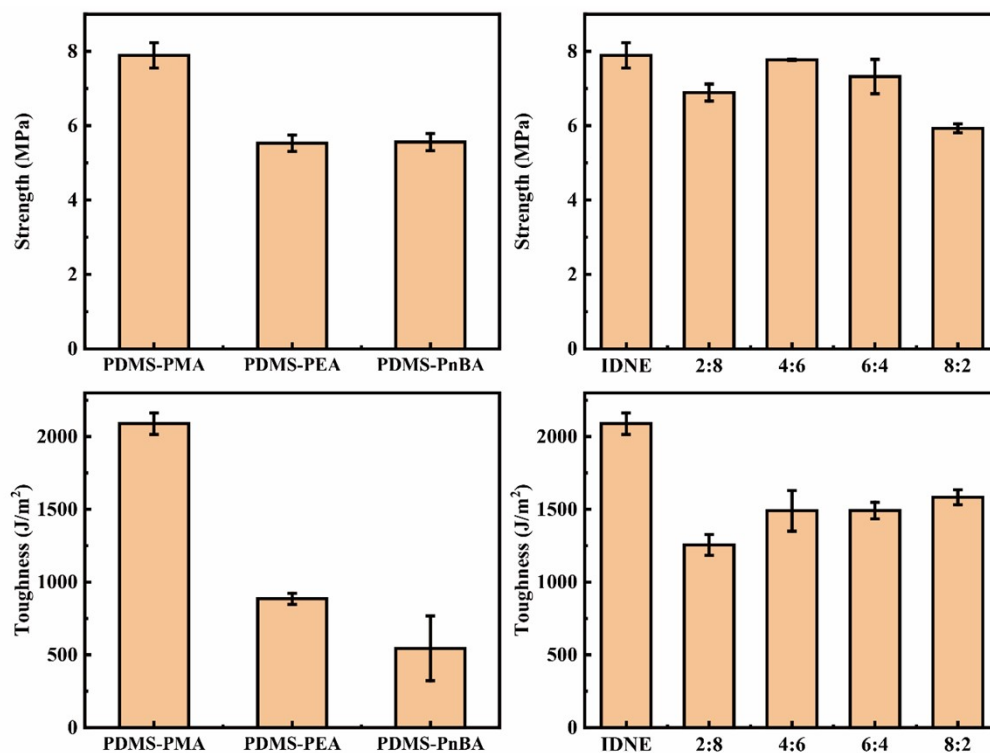


Figure. S9. S-S curve of PDMS and IDNE with pre-crack in different double network structure and ratios